Journal of Hepatocellular Carcinoma

Dovepress
Taylor & Francis Group

Open Access Full Text Article

ORIGINAL RESEARCH

Prognostic Significance and Mechanistic Insights of Rutin-Related Ferroptosis Gene Signature in Hepatocellular Carcinoma

Weifeng Yao[1,*], Hui Li[2,*], Yongle Zhang[1], Xufen Xia[1], Hai Wang[1], Zhen Zhang[1], Danfang Shi[1]

[1]Department of Clinical Laboratory, Tongde Hospital of Zhejiang Province, Hangzhou, People's Republic of China; [2]Key Laboratory of Neuroregeneration of Jiangsu and Ministry of Education, Co-Innovation Center of Neuroregeneration, Medical School of Nantong University, Nantong University, Nantong, People's Republic of China

*These authors contributed equally to this work

Correspondence: Danfang Shi, Department of Clinical Laboratory, Tongde Hospital of Zhejiang Province, Hangzhou, People's Republic of China, Email 1830927743@qq.com

Purpose: This study aims to elucidate the anti-tumor properties of rutin and its specific molecular mechanisms for inhibiting hepatocellular carcinoma (HCC) through the ferroptosis.

Methods: The effects of rutin on HuH-7 cell proliferation, migration, invasion, and cell cycle progression were evaluated through in vitro experiments. By integrating bioinformatics analysis and network pharmacology, potential ferroptosis targets influenced by rutin in HCC were identified from the TCGA-LIHC database. A prognosis-related risk-scoring model was constructed and validated in the GEO14520 cohort and ICGC-LIRI-JP. Samples were categorized into high-risk and low-risk groups based on their scores. Enriched pathways within these different risk groups were explored using Gene Set Enrichment Analysis (GSEA) and Gene Set Variation Analysis (GSVA). Additionally, key targets of rutin-related ferroptosis in HCC cells were investigated through single-cell analysis and molecular docking studies.

Results: Rutin inhibited the proliferation, invasion, migration, and cell cycle progression of HCC cells in a dose-dependent manner. We constructed a risk model comprising five ferroptosis-related targets of rutin (FRTs-R): ACACA, AKR1C3, ALDH2, AR, and CDK1. This prognostic model was validated in the GEO14520 and ICGC datasets, revealing that the low-risk group had a better prognosis than the high-risk group. Furthermore, lipid metabolism pathway activity was up-regulated in the low-risk group. Single-cell analysis indicated specific expression of AKR1C3 in HCC cells, while molecular docking analysis showed that, among the five potential targets, AKR1C3 demonstrated the most stable binding affinity to rutin.

Conclusion: Our findings suggest that rutin may modulate ferroptosis in HCC, with rutin associated ferroptosis genes implicated in disease biology; moreover, the proposed risk scoring model shows promising prognostic utility in HCC.

Keywords: hepatocellular carcinoma, rutin, ferroptosis, bioinformatics, in vitro experiment

Introduction

Hepatocellular carcinoma (HCC) ranks as the sixth most common malignancy globally and is the third leading cause of cancer-related deaths,[1] with a dismal 5-year survival rate of only 10.1% for patients with advanced stages.[2] The aggressive nature and rapid progression of HCC make its overall prognosis poor, posing a significant threat to global health. Traditional treatments such as surgery, radiotherapy, and chemotherapy are often hampered by high costs, severe side effects, and the development of drug resistance, which reduces their effectiveness, especially in advanced liver cancer.[3] Furthermore, immune checkpoint inhibitors (ICIs) in combination with bevacizumab, ICIs combined with tyrosine kinase inhibitors (TKIs), and dual immunotherapy can significantly enhance overall survival in patients with advanced HCC.[4] However, these treatments also encounter several challenges, including low overall response rates, widespread drug resistance, and a high incidence of adverse drug reactions,[5] emphasizing the urgent need for novel therapeutic strategies and new molecular targets.

Received: 14 August 2025
Accepted: 6 December 2025
Published: 23 December 2025

Comprehensive research into the pathogenesis of HCC and the development of innovative treatment options could address existing therapeutic bottlenecks and significantly improve patient outcomes.

Natural products are increasingly recognized for their potential in developing novel chemotherapeutic agents.[6] Rutin, a glycoside composed of a flavonoid and the disaccharide rutinose, is abundantly found in a variety of plants, including apples, passion fruit, tea, and buckwheat. Numerous studies have demonstrated that rutin exhibits a wide range of pharmacological activities, including anti-inflammatory, antioxidant, antidiabetic, vasoprotective, antibacterial, and anticancer properties.[7,8] In various in vitro models, rutin has been shown to inhibit tumor growth, including that of hepatocellular carcinoma and human neuroblastoma, and to induce cell cycle arrest and apoptosis.[9,10] Notably, rutin can enhance the sensitivity of HCC cells to Sorafenib by suppressing autophagy through inhibition of BANCR expression and modulation of the BANCR/miRNA-590-5p/OLR1 axis.[11] Despite these promising findings, the precise mechanisms through which rutin exerts its anticancer effects in HCC remain poorly understood, and few studies systematically utilize bioinformatics to identify its key anti-tumor targets and molecular mechanisms.

Ferroptosis is a novel form of regulated cell death that is distinct from traditional apoptosis and necrosis, closely linked to dysregulation of iron metabolism and increased intracellular lipid peroxidation. Research indicates that ferroptosis can inhibit HCC progression and plays a crucial role in cancer therapy.[12] The cellular susceptibility to ferroptosis is associated with multiple metabolic pathways, notably fatty acid metabolism. The synthesis and activity of polyunsaturated fatty acids govern the accumulation of phospholipid hydroperoxides; exceeding a certain threshold of these hydroperoxides in HCC cells can trigger ferroptosis. Therefore, a detailed investigation of the mechanisms underlying ferroptosis in HCC may uncover novel therapeutic targets for intervention.

Current research on rutin and ferroptosis has predominantly focused on non-neoplastic conditions (eg, spinal cord injury,[13] ulcerative colitis,[14] and ventilator induced lung injury[15]), whereas studies in HCC remain scarce. Canonical ferroptosis inducers, such as erastin and RSL3, effectively trigger tumor-cell death but can also impair antitumor immune responses and cause hepato- and nephrotoxicity.[16,17] In contrast, rutin has been reported in vitro and in vivo to alleviate hepatotoxicity and modulate immune-cell proportions, including increases in specific subsets,[18,19] suggesting potential advantages for regulating ferroptosis in HCC while balancing efficacy and safety relative to canonical inducers. Based on the above premises, this study utilizes the HuH-7 cell line as a model to explore the inhibitory effects of rutin on liver cancer cells. Furthermore, bioinformatics and network pharmacology will be employed to dissect the potential molecular mechanisms of rutin-related ferroptosis in HCC. The findings aim to provide a scientific basis for applying rutin in liver cancer treatment and contribute to the development of novel anti-liver cancer therapies.

Materials and Methods

Materials and Antibodies

Rutin (purity 97.19%, T0795) was purchased from TargetMol (Boston, MA, USA). Penicillin-Streptomycin solution (P1400), 0.25% Trypsin (T1300-100), and Phosphate Buffered Saline (PBS, P1022) were obtained from Solarbio (Beijing, China). Dulbecco's Modified Eagle Medium (DMEM, BL304A) was purchased from Biosharp (Anhui, China), and Fetal Bovine Serum (FBS, 35–081-CV) was sourced from CORNING (New York, USA). The EdU Cell Proliferation Kit (C0071S) and TUNEL Apoptosis Detection Kit (C1088) were both obtained from Beyotime Biotechnology (Shanghai, China).

Cell Culture

Human hepatocellular carcinoma HuH-7 cells were obtained from Procell (Wuhan, China). The cells were cultured in Dulbecco's Modified Eagle Medium (DMEM) supplemented with 10% fetal bovine serum (FBS) and 1% penicillin-streptomycin solution. Cells were maintained in a humidified incubator (Thermo Forma 3111) at 37°C with 5% CO_2. The cells were passaged every 2 to 3 days to ensure they remained in the logarithmic growth phase for subsequent experiments.

EdU Assay for Cell Proliferation

We generated 48 hour dose response curves in normal liver cells (L02) and Huh-7 and estimated IC50 values using a four parameter logistic fit. The IC50 values were 37.14 μmol/L for L02 (Supplementary Figure 1A) and 8.48 μmol/L for Huh-7

(Supplementary Figure 1B). Guided by the Huh-7 IC50 and the tolerance window of normal liver cells, we selected rutin concentrations of 0, 10, and 40 μmol/L. HuH-7 cells were seeded at a density of 3×10^4 cells/well in a 24-well plate and cultured at 37°C for 48 hours in a medium containing different concentrations of rutin (0, 10, and 40 μmol/L). Cell proliferation was assessed using the EdU cell proliferation assay kit. Following 2 hours of incubation with EdU, cells were fixed with 4% paraformaldehyde for 15 minutes, washed three times with PBS, and then permeabilized with 0.3% Triton X-100 for 10 minutes. After three additional washes with PBS, the Click reaction cocktail was prepared according to the manufacturer's instructions, and 100 μL was gently added to each well. The cells were incubated at room temperature in the dark for 30 minutes, washed three times with PBS, and then stained with Hoechst 33342 at a dilution of 1:1000 for 10 minutes, followed by three more washes with PBS. Finally, the slides were mounted and observed under a fluorescence microscope, where cell nuclei appeared blue and positive results appeared green.

Transwell Assay for Cell Migration

HuH-7 cells were treated with various concentrations of rutin (0, 10, and 40 μmol/L) and incubated for 48 hours in a CO_2 incubator. Subsequently, 0.7 mL of complete medium was added to each well of a 24-well plate, and the Transwell inserts were placed into each well to soak. After harvesting the cells via trypsin digestion, the cells were washed with basal medium and resuspended. The cell density was adjusted to 5×10^4 cells/mL, and 0.3 mL of the cell suspension was added to each insert (with three replicates per group) and incubated in a 37°C incubator for 48 hours. Following incubation, 1 mL of 4% paraformaldehyde solution was added to each well and allowed to fix at room temperature for 15 minutes. After fixation, the fixative was aspirated, and the wells were washed once with PBS. Then, 1 mL of 0.1% crystal violet solution was added for staining for 3 minutes. Subsequently, the wells were washed three times with PBS, and excess liquid was removed. Finally, the non-migrated cells inside the Transwell inserts were carefully wiped off with a cotton swab, and the remaining cells were observed under a 100× microscope. The number of cells in each field of view was counted and subjected to statistical analysis.

Cell Cycle Analysis by Flow Cytometry

HuH-7 cells were treated with various concentrations of rutin (0, 10, and 40 μmol/L) and incubated for 48 hours in a CO_2 incubator. Following trypsin digestion, the cells were resuspended to create a single-cell suspension and fixed with absolute ethanol for 48 hours. The cells were then resuspended in PBS. Each cell sample was incubated with 500 μL of staining buffer, 10 μL of RNase A, and 25 μL of propidium iodide solution for 30 minutes at 37°C in the dark to stain the nuclei. After staining, the samples were analyzed by flow cytometry within 48 hours. Red fluorescence was detected at an excitation wavelength of 488 nm, corresponding to the FL2 detection channel of the flow cytometer, while light scatter was recorded simultaneously. Cell cycle analysis was conducted using FLOWJO software.

Acquisition of Ferroptosis-Related Rutin Intervention Targets

The structure of rutin was obtained from the PubChem database by searching for "rutin" and downloading its SMILES string and 3-dimensional structure. Rutin targets were identified using PharmMapper (task ID: 250516042715), SwissTarget, and TargetNet. After removing duplicates, the target names were standardized to gene names using the UniProt database. Ferroptosis-related genes (FRGs) were sourced from the FerrDb database. Differential analysis of the GSE14520 Cohort 1 dataset (Normal = 41 vs Tumor = 41) from the Gene Expression Omnibus (GEO) database was conducted using the limma package in R. Transcriptome data were log2-transformed and normalized for quality assessment; box plots and principal component analysis were applied. Differentially expressed genes (DEGs) in HCC were identified using criteria of $P < 0.05$ and $|\log2 \text{ fold change}| > 1$. Data from rutin targets, FRGs, and DEGs were integrated and analyzed in R to identify unique and shared targets. Visualization of this data was performed using the ggplot2 and Venn-Diagram packages, leading to the identification of ferroptosis-related targets of rutin (FRTs-R). Gene expression data for HCC patients from The Cancer Genome Atlas Liver Hepatocellular Carcinoma (TCGA-LIHC) cohort were obtained from the TCGA database (https://portal.gdc.cancer.gov/). Additionally, gene expression data for HCC patients from the JP Project of the International Cancer Genome Consortium (ICGC-LIRI-JP) were accessed from the ICGC database (https://dcc.icgc.org/).

Prognostic Analysis and Nomogram Construction of FRTs-R

RNA sequencing (RNAseq) and clinical data from the TCGA-LIHC cohort were curated, with samples lacking clinical information excluded from the analysis. A total of five genes were selected for further analysis using univariate Cox regression and Lasso regression to identify those most associated with HCC prognosis, with cross-validation ensuring the robustness of the findings. The glmnet package in R (version 4.2.1) was utilized for data analysis and visualization. The genes significantly correlated with prognosis—acetyl CoA carboxylase 1 (ACACA), human aldo-keto reductase family 1 member C3 (AKR1C3), aldehyde dehydrogenase 2 (ALDH2), androgen receptor (AR), and cyclin-dependent kinase 1 (CDK1)—were further analyzed using multivariate Cox regression models to calculate risk scores based on survival outcomes from the TCGA-LIHC cohort (Tumor samples = 336; training cohort). The timeROC package was employed to assess the predictive efficacy of these scores for 1-year, 3-year, and 5-year survival. Patients were stratified into high-risk and low-risk groups based on median risk scores, and survival outcomes were compared using Log rank tests and Kaplan-Meier curves. Subsequently, transcriptomic data from ICGC-LIRI-JP (Tumor samples = 232; validation cohort 1) and microarray gene expression data from GSE14520 (Tumor samples = 169; validation cohort 2) were used to validate the risk score model.

A nomogram model was constructed using the rms and survival packages in R, integrating risk scores and clinical data to predict 1-year, 3-year, and 5-year survival. Calibration analysis was performed to validate the predictive performance of the nomogram.

Functional Strengthens of the Two Risk Groups

DEGs between the low-risk and high-risk groups were identified using the DEGseq R package. Genes with an absolute log2 fold change greater than 1 and a significance threshold of $P < 0.05$ were considered DEGs. Gene ontology (GO) analysis and Kyoto Encyclopedia of Genes and Genomes (KEGG) pathway analysis were performed on the identified DEGs to assess their functional categorization and pathways involved. Additionally, Gene Set Enrichment Analysis (GSEA) was conducted to identify significantly enriched functional characterizations within the two risk groups. To evaluate potential biological function changes in the different risk groups, the Gene Set Variation Analysis (GSVA) algorithm was employed to comprehensively score each gene set.

Analysis of Immune Cell Infiltration and Immune Checkpoint Expression on the Two Risk Groups

The CIBERSORT algorithm was used to analyze the RNA-seq data from the different risk groups to infer the relative proportions of 22 immune infiltrating cell types. Additionally, the expression levels of immune checkpoint genes were compared between the two risk groups; a P-value of < 0.05 was considered statistically significant.

Drug Sensitivity Analysis

Using the pRRophetic R package, we conducted broad drug screening based on the GDSC database (https://www.sanger.ac.uk/tool/gdsc-genomics-drug-sensitivity-cancer/) to identify the drug agents that the two risk groups may respond to sensitively.

Single-Cell RNA-Sequencing Data Analysis

About 109346 high-quality cells were filtered and obtained from the LIHC_GSE189903 dataset. The expression pattern of the key FRTs-R were visualized by the Seurat R package based on the single-cell profile of LIHC_GSE189903. Approximately 27,989 high-quality cells were obtained after filtering the GSE149614 dataset. Using the single-cell profiles from GSE149614, we visualized the expression patterns of key FRTs-R with the Seurat R package.

Validation of the protein Expression Levels of the key Genes Via the human Protein Atlas

To further validate the protein expression levels of ACACA, AKR1C3, ALDH2, AR, and CDK1 in liver cancer and normal tissues, we downloaded immunohistochemistry (IHC) data from the Human Protein Atlas (HPA, http://www.proteinatlas.org). The HPA provides IHC results for numerous proteins across various cancer and normal tissues.

Molecular Docking

Molecular docking was used to evaluate the binding of rutin to intervention target proteins. The 3dimensional molecular structure of rutin in SDF format was obtained from the PubChem database (https://pubchem.ncbi.nlm.nih.gov/). The X-ray crystal structure files of ACACA, AKR1C3, ALDH2, AR and CDK1 proteins were obtained from the RCSB Protein Data Bank (http://www.rcsb.org/). The proteins were processed to remove water molecules and were properly hydrogenated before being saved in PDB format. Docking studies between rutin and the proteins ACACA, AKR1C3, ALDH2, AR, and CDK1 were conducted using AutoDock 1.5.6 and visualized with PyMOL 3.1.5.1. The grid box feature of the AutoDock tool was utilized to define the specific binding pocket of rutin within the active site of the proteins. Subsequently, molecular docking analyses were performed via the command prompt, and the results were visualized using PyMOL.

Statistical Analysis

All statistical analyses were performed using R (version 4.4.2). $P < 0.05$ was considered statistically significant. "*" indicates $P < 0.05$, "**" indicates $P < 0.01$, "***" indicates $P < 0.001$ and "****" indicates $P < 0.0001$ throughout this study.

Results

Inhibition of HCC Cell Proliferation, Migration, Cell Cycle Progression, and Induction of Apoptosis by Rutin

The inhibitory effect of rutin on HuH-7 cell proliferation was assessed using an EdU assay. Treatment with 10 and 40 μmol/L rutin for 48 hours significantly reduced the number of EdU-labeled proliferating cells compared to the control group, demonstrating statistically significant differences ($P < 0.01$) (Figure 1A and B). These findings confirm that rutin inhibits HuH-7 cell proliferation in a dose-dependent manner.

To further investigate the effect of rutin on HuH-7 cell migration, we performed a transwell migration assay. The results demonstrated a significant reduction in the number of migrated cells in the treatment groups compared to the control group. Specifically, at rutin concentrations of 10 μmol/L and 40 μmol/L, the number of cells migrating to the lower chamber was significantly lower than that in the control group ($P < 0.01$), indicating that rutin effectively inhibits HuH-7 cell migration at these concentrations (Figure 2A and B).

To determine whether rutin inhibits cell proliferation by affecting the HuH-7 cell cycle, we conducted flow cytometric cell cycle analysis. The results indicated that the proportion of cells in the G1 phase was significantly higher in the 10 μmol/L and 40 μmol/L rutin treatment groups than in the control group ($P < 0.0001$ and $P < 0.001$). Conversely, the proportion of cells in the G2 phase was significantly lower in both the 10 μmol/L and 40 μmol/L rutin treatment groups compared to the control group ($P < 0.05$ and $P < 0.01$) (Figure 2C and D). These findings suggest that rutin treatment significantly alters the cell cycle distribution of HuH-7 cells and may inhibit cell proliferation by regulating the cell cycle.

Acquisition and Expression Analysis of Rutin Intervention Targets in HCC Patients

A total of 299 targets were identified from PharmMapper, 102 from SwissTarget, and 618 from TargetNet. Using the UniProt database, all targets were converted into their corresponding gene names, resulting in 624 potential rutin-targeted genes (RTGs) after removing duplicates. Additionally, 2264 FRGs were identified from the FerrDb database. Differential analysis was conducted using the limma package with a threshold of $P < 0.05$ and $|\log2 \text{ fold change}| > 1$. In the GSE14250 Cohort 1 dataset, 962 DEGs were identified, with 614 downregulated and 348 upregulated in HCC samples (Figure 3A). R was used to analyze unique and overlapping targets among the groups, revealing 15 FRTs-R: Acetyl-CoA Carboxylase Alpha (ACACA), Aldo-Keto Reductase Family 1 Member C3 (AKR1C3), Aldehyde Dehydrogenase 2 (ALDH2), Androgen Receptor (AR), Aurora Kinase A (AURKA), AXL Receptor Tyrosine Kinase (AXL), Cyclin Dependent Kinase 1 (CDK1), Dihydroorotate Dehydrogenase (DHODH), Estrogen Receptor 1 (ESR1), Histone Deacetylase 6 (HDAC6), Mitogen-Activated Protein Kinase 9 (MAPK9), Microsomal Triglyceride Transfer Protein (MTTP), Platelet-Derived Growth Factor Receptor Alpha (PDGFRA), Squalene Epoxidase (SQLE), and Transient Receptor Potential Cation Channel Subfamily V Member 1 (TRPV1) (Figure 3B). Among the 15 FRTs-R, univariate

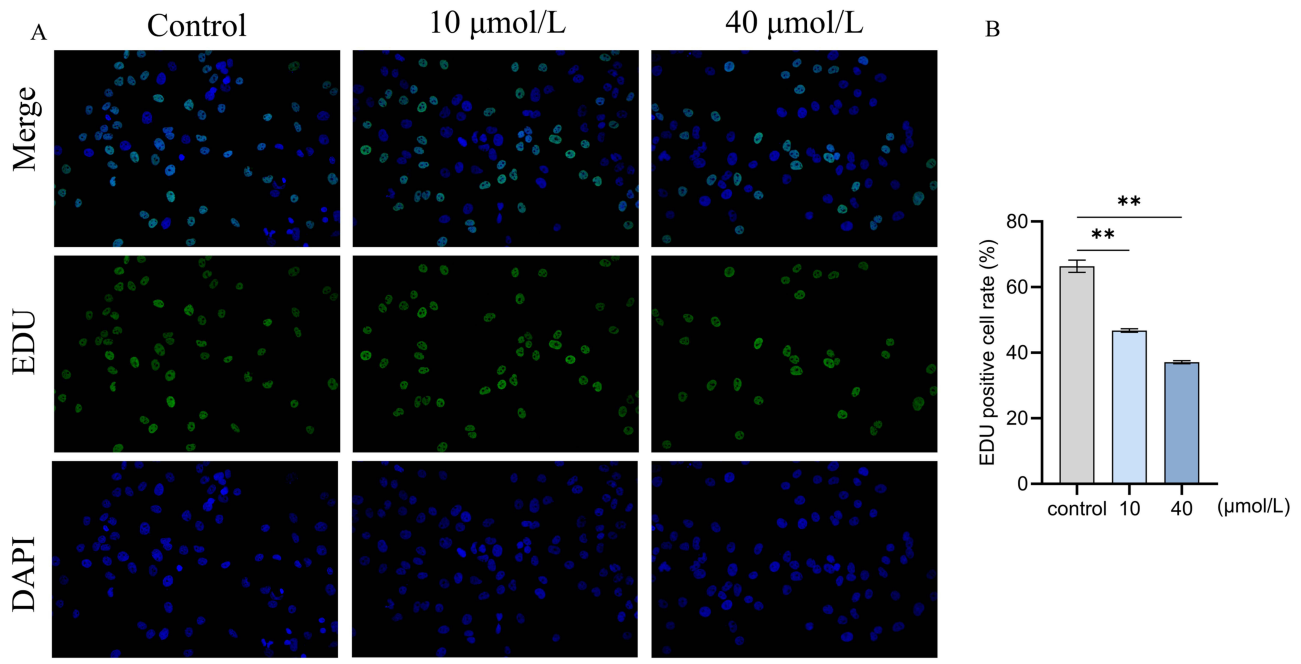

Figure 1 Rutin inhibits HuH-7 cell proliferation. (**A** and **B**) Cell proliferation of HuH-7 cells measured by EdU assay. Data are presented as the mean ± SEM of three independent experiments. " **" indicates $P < 0.01$ compared to the control group.

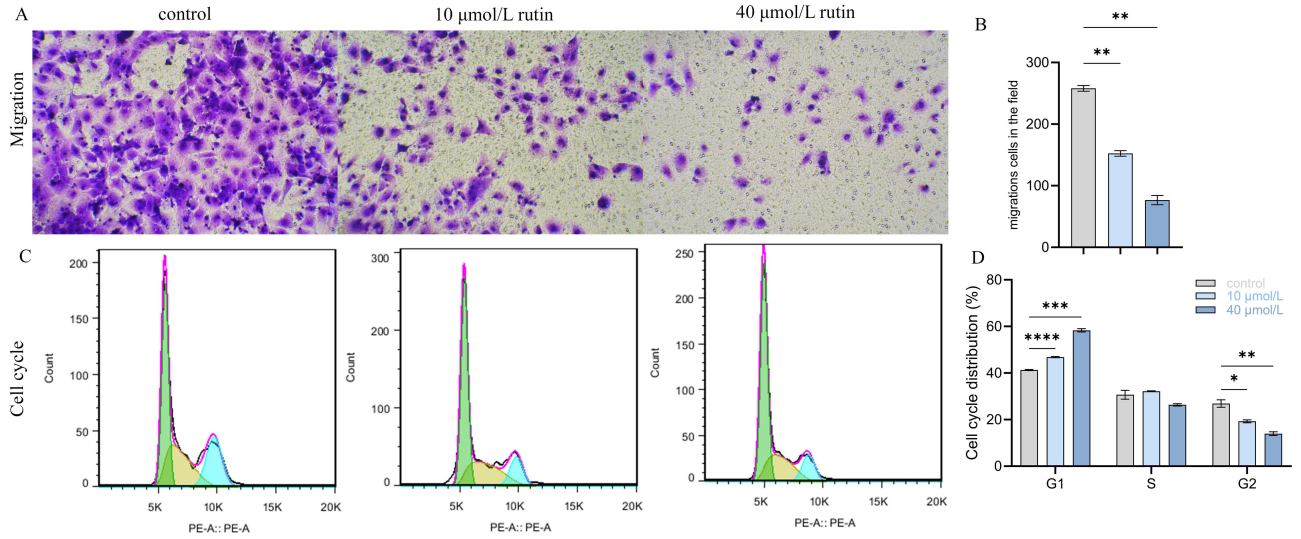

Figure 2 Rutin inhibits HuH-7 cell migration and cell cycle progression (mean ± SD, n = 3). (**A** and **B**) Transwell assay (× 100 magnification) to evaluate the migration ability of HuH-7 cells; (**C** and **D**) Flow cytometry assay to evaluate the proliferation ability and cell cycle regulation of HuH-7 cells. "*" indicates $P < 0.05$, "**" indicates $P < 0.01$, "***" indicates $P < 0.001$ and "****" indicates $P < 0.0001$ compared to the control group (0 μmol/L Rutin).

COX regression analysis in the TCGA-LIHC cohort selected genes with a $P < 0.05$: ACACA, CDK1, AKR1C3, AURKA, ESR1, AR, DHODH, and ALDH2. Lasso regression with ten-fold cross-validation identified the key FRTs-R—ACACA, AKR1C3, AR, ALDH2, and CDK1—as having the strongest correlation with rutin-related ferroptosis and HCC patient prognosis. This analysis yielded variable lambda values and maximum likelihood estimates, which were visualized (Figure 3C and D). Five genes exhibited differential expression in the GSE14250 Cohort 1 and TCGA HCC tissues (Figure 3E and F), with three genes (ACACA, AKR1C3, and CDK1) upregulated in HCC tissues ($P < 0.0001$) and two genes (ALDH2 and AR) downregulated ($P < 0.0001$).

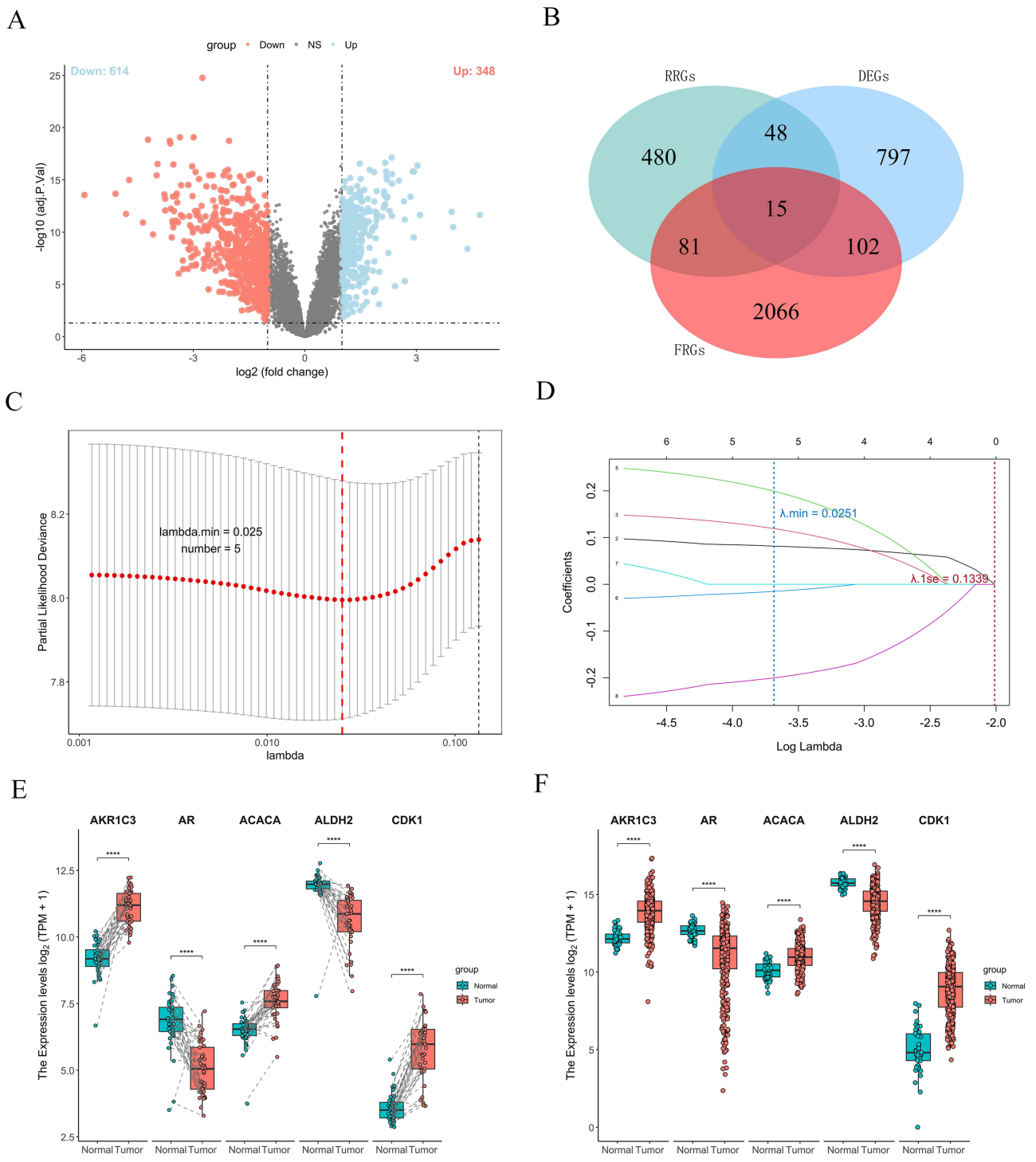

Figure 3 Acquisition and expression difference of rutin intervention targets. (**A**) Volcano plot representing differential analysis based on the GSE14520 Cohort 1 dataset. (**B**) Venn diagram illustrating the intersection of rutin-targeted genes (RTGs), differentially expressed genes (DEGs) from the GSE14520 Cohort 1 dataset and ferroptosis-related genes (FRGs). (**C** and **D**) Lasso regression analysis of rutin intervention targets. (**E**): Paired expression analysis of rutin intervention targets in the GSE14520 Cohort 1 dataset. (**F**) Unpaired expression analysis of rutin intervention targets in TCGA-LIHC patients. "****" indicates $P < 0.0001$.

Abbreviations: NS, Not significant; FRGs, Ferroptosis-related genes; RTGs, Rutin-related genes; DEGs, Differentially expressed genes; ACACA, Acetyl-CoA Carboxylase Alpha; AKR1C3, Aldo-Keto Reductase Family 1 Member C3; ALDH2, Aldehyde Dehydrogenase 2; AR, Androgen Receptor; CDK1, Cyclin-Dependent Kinase 1.

https://doi.org/10.2147/JHC.S560755

We compared baseline distributions of sex, age, and tumor–node–metastasis (TNM) stage between the TCGA-LIHC training cohort and the ICGC-LIRI-JP and GSE14250 external validation cohorts. Baseline characteristics differed across the three cohorts (Table 1). This heterogeneity facilitates evaluation of the robustness and generalizability of prognostic models across diverse clinical settings.

Prognostic Analysis and Nomogram Construction of the Key Ferroptosis-Related Target of Rutin in HCC Patients

A Cox proportional hazards model was developed using multivariate Cox regression analysis to calculate correlation coefficients and risk values based on the expression of key ferroptosis-related targets of rutin. The prognostic efficacy of this five-gene risk scoring system was evaluated using time-dependent receiver operating characteristic curves for 1-year, 3-year, and 5-year survival, demonstrating predictive value in both the TCGA-LIHC and GSE14250 Cohort 1 datasets (Figure 4A and B). Due to the absence of patients with survival times of 5 years or more in the ICGC-LIRI-JP cohort, only the 1-year and 3-year AUC curves are presented (Figure 4C). Based on the median risk score, patients in the TCGA-LIHC cohort were classified into high-risk (168 patients) and low-risk (168 patients) groups. The high-risk group exhibited significantly poorer survival ($P = 0.0004$), indicating that the five-gene risk score effectively predicts prognosis (Figure 4D). This model was further validated in the GSE14250 Cohort 1 and ICGC-LIRI-JP cohorts, which also demonstrated that the five-gene risk score effectively predicts the prognosis of HCC patients ($P = 0.006$ and $P = 0.0024$) (Figure 4E and F).

Univariate and multivariate Cox regression analyses were performed on the risk scores and clinical information of HCC patients. The univariate analysis identified the TNM stage and risk score as significant prognostic factors ($P < 0.001$) (Figure 5A). Subsequent multivariate analysis revealed that TNM stage and risk score were independent prognostic factors, as illustrated in a forest plot (Figure 5B). To further enhance prognostic predictions, a nomogram incorporating age, TNM stage, race, gender, and risk score was constructed to estimate 1-year, 3-year, and 5-year survival. The nomogram achieved a concordance index of 0.662, indicating good predictive accuracy (Figure 6).

Calibration analysis demonstrated that the nomogram's predictions for 1-year, 3-year, and 5-year survival closely aligned with observed outcomes, thereby supporting the model's prognostic validity (Figure 7A–C). Additionally, decision curve analysis revealed that the nomogram developed in this study provided greater net benefits compared to traditional models at the 1-year, 3-year, and 5-year follow-up time points (Figure 7D–F).

Substance Metabolism Activities Were Strengthened in Low-Risk Group

First, DEGs between the low-risk and high-risk groups were identified. The DEGs from each risk group underwent GSEA to assess functional enrichment. The biological activities significantly enriched in the high-risk group included positive regulation of the cell cycle, DNA replication, homologous recombination, ribosome activity, spliceosome function, DNA replication initiation, DNA unwinding during replication, kinetochore assembly, kinetochore organization, and outer

Table 1 Pairwise Comparisons of Baseline Characteristics Across the TCGA-LIHC, ICGC-LIRI-JP, and GSE14250 Cohort 1 Datasets.

	TCGA-LIHC (N=336)	ICGC-LIRI-JP (N=232)	GSE14250 Cohort 1 (N=169)	*P*-Value[a]	*P*-Value[b]
Age (mean (SD))	59.78 (13.08)	67.25 (10.13)	51.22 (10.44)	<0.001	<0.001
Sex (%)					
Male	228 (67.9)	171 (73.7)	147 (87.0)	0.160	<0.001
Female	108 (32.1)	61 (26.3)	22 (13.0)		
TNM stage (%)					
Uncertain	23 (6.8)	0 (0.0)	2 (1.2)	<0.001	0.001
I	156 (46.4)	36 (15.5)	75 (44.4)		
II	73 (21.7)	106 (45.7)	60 (35.5)		
III	80 (23.8)	71 (30.6)	32 (18.9)		
IV	4 (1.2)	19 (8.2)	0 (0.0)		

Note: [a]TCGA-LIHC Versus ICGC-LIRI-JP; [b]TCGA-LIHC Versus GSE14250 Cohort 1.

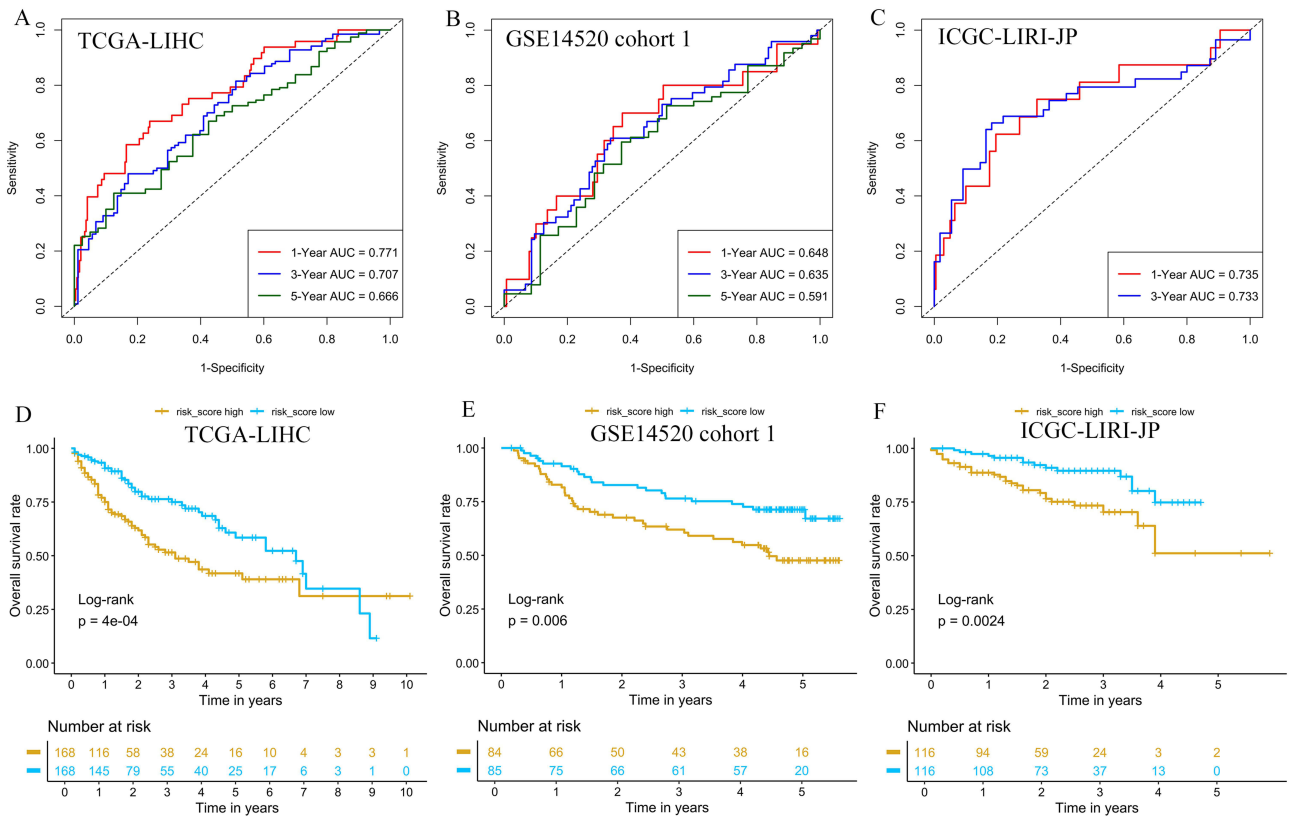

Figure 4 Evaluation of the risk assessment system for rutin intervention targets. (**A-C**) Time-receiver operating characteristic curve of the risk assessment system in TCGA-LIHC, GSE14520 cohort 1 and ICGC-LIRI-JP datasets; (**D–F**) Kaplan-Meier curve comparing the survival between high- and low-risk groups in TCGA-LIHC, GSE14520 cohort 1 and ICGC-LIRI-JP datasets.

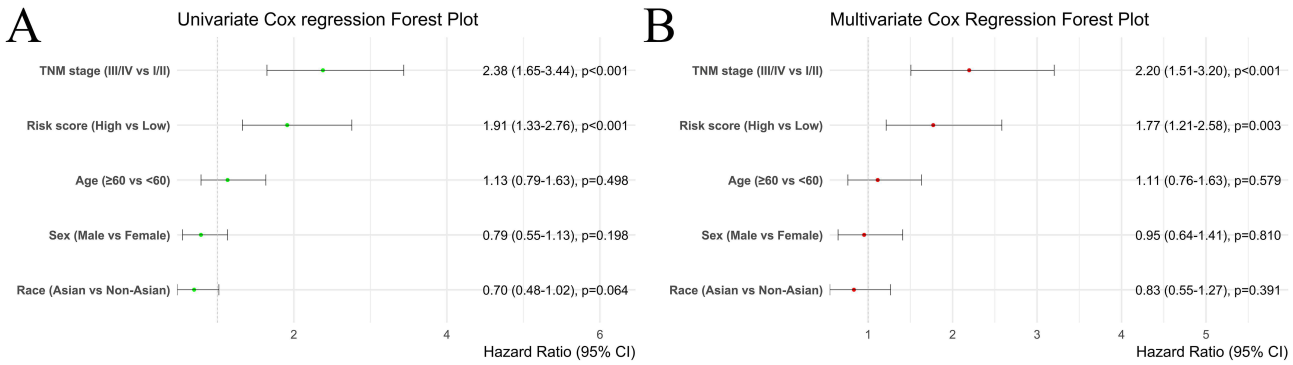

Figure 5 Univariate and multivariate Cox analyses for the independent prognostic factors for HCC in the TCGA-LIHC. (**A**) Forest plot of univariate Cox regression analysis of risk score, TNM stage, age, gender and race. (**B**) Forest plot of multivariate Cox regression analysis of risk score and TNM stage.
Abbreviations: HR, Hazard ratios; CI, Confidence intervals.

kinetochore assembly (Figure 8A and B). In contrast, the biological activities significantly enriched in the low-risk group encompassed beta-oxidation, bile acid biosynthesis, isoleucine degradation, lectin pathway of the coagulation cascade (fibrinogen to fibrin), lectin pathway of the complement cascade (C4 and C2 to C3 convertase), fatty acid beta-oxidation, fatty acid catabolism, xenobiotic catabolism, microorganism lumen, and oxidoreductase activity acting on paired donors, reduced by the incorporation or reduction of molecular oxygen (Figure 8C and D). GSVA indicated that metabolic activity was relatively stronger in the low-risk group, suggesting that metabolic processes are significantly enhanced in this group (Figure 8E and F). In conclusion, both GSEA and GSVA indicate that metabolic activities are more pronounced in the low-risk group compared to the high-risk group.

https://doi.org/10.2147/JHC.S560755

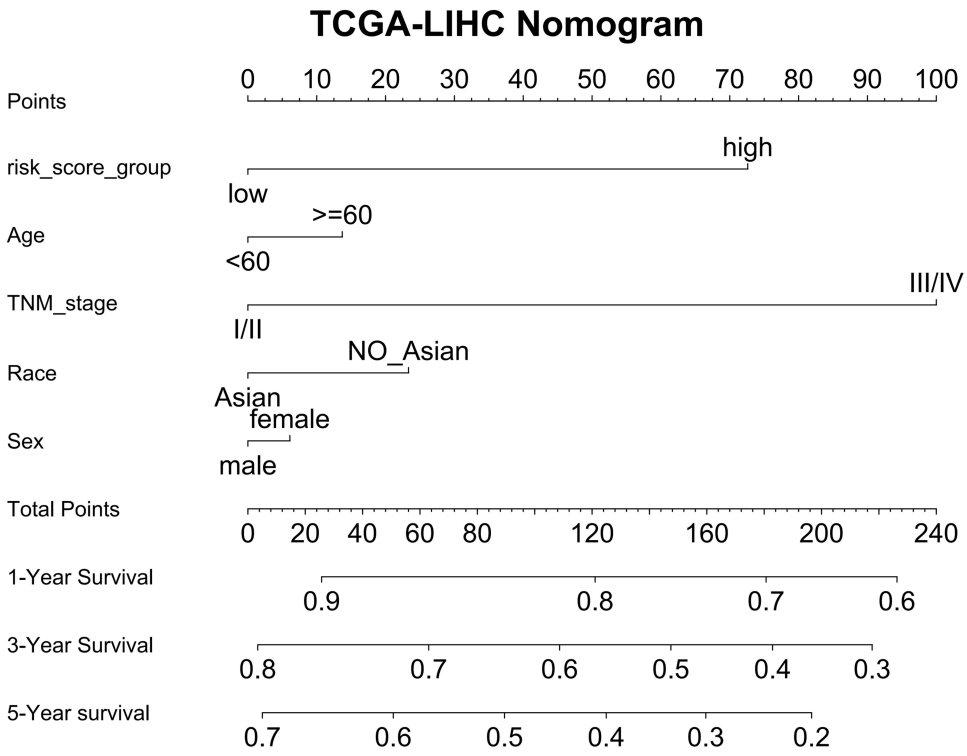

Figure 6 Construction of nomogram integrating risk score and clinical information.

Exploring Immunobiological Characteristics and Their Clinical Value Across Different Risk Groups from Multiple Perspectives

To further investigate the immunobiological characteristics of FRTs-R across different risk groups, we analyzed immune cell infiltration and the correlation between key FRTs-R and immune cells. In the high-risk group, the proportions of B memory cells, activated CD4 memory T cells, follicular helper T cells, regulatory T cells (Tregs), M0 macrophages, and resting dendritic cells were significantly higher than those in the low-risk group. Conversely, the proportions of resting mast cells and monocytes were lower in the high-risk group (Figure 9A). Additionally, we observed a higher M1/M2 macrophage ratio in the low-risk group ($P = 0.053$). We found that AKR1C3 was significantly positively correlated with M2 macrophages and Tregs, while it was negatively correlated with naive B cells. CDK1 displayed a significant positive correlation with follicular helper T cells and a significant negative correlation with monocytes. Furthermore, AR was positively correlated with monocytes and negatively correlated with Tregs. ALDH2 showed a significant positive correlation with monocytes and a significant negative correlation with Tregs as well. In contrast, ACACA had a significant positive correlation with resting dendritic cells and follicular helper T cells, along with a significant negative correlation with resting CD4 memory T cells (Figure 9B). We analyzed differences in immune checkpoint expression between the two risk groups, focusing on PD-1, CTLA-4, TIM3, LAG3, TIGIT, and B7-H3. The results indicated that immune checkpoint expression levels were higher in the high-risk group (Figure 9C). For drug sensitivity predictions, we utilized the R package "pRRophetic", which predicts tumor patients' responses to chemotherapy drugs based on gene expression profiles. Our analysis revealed that the high-risk group was more sensitive to Etoposide and Sunitinib, while the opposite was observed for Erlotinib and Lapatinib (Figure 9D). In summary, the risk model established for HCC tumors based on FRTs-R is associated with the infiltration status of immune cells in the tumor microenvironment. This model may aid in selecting immune checkpoint inhibitors and chemotherapy drugs for patients with hepatocellular carcinoma.

Single-Cell Profiling of Key FRTs-R in the Tumor Microenvironment of LIHC

To further investigate the expression patterns of key FRTs-R in the LIHC tumor microenvironment (TME), we conducted a single-cell profiling study. The single-cell annotation map of the LIHC_GSE189903 dataset is presented in Figure 10A.

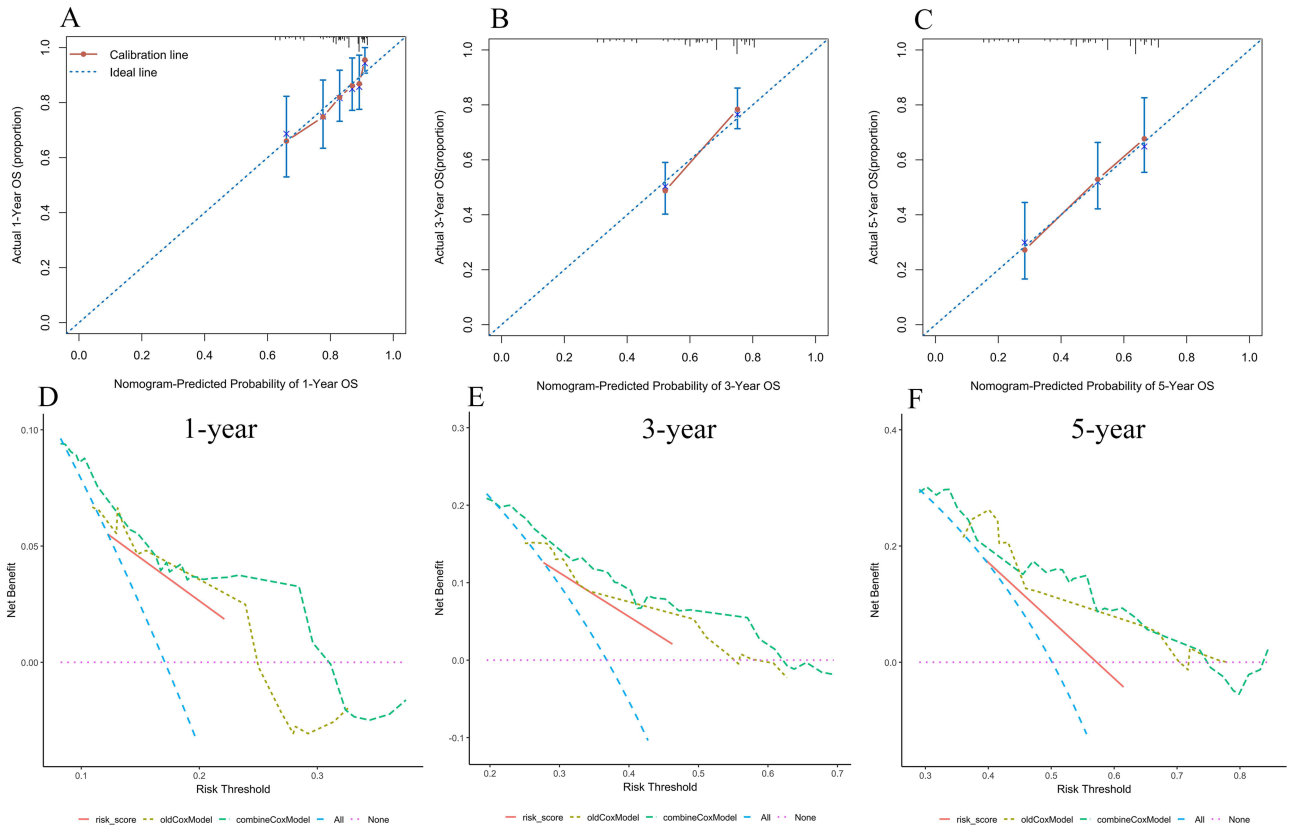

Figure 7 Evaluation of nomogram. (**A**–**C**) Calibration plots of the nomogram for 1-year, 3-year, and 5-year survival; (**D**–**F**) decision curve analysis curves of the nomogram for 1-year, 3-year, and 5-year.

Our analysis revealed that within the tumor microenvironment (TME), ALDH2 is predominantly expressed in monocytes, fibroblasts, and hepatocytes, while AKR1C3 is primarily expressed in hepatocytes. In contrast, AR, ACACA, and CDK1 did not exhibit significant expression in monocytes, fibroblasts, B cells, endothelial cells, hepatocytes, or NK cells (Figure 10B–K). These findings suggest that AKR1C3 and ALDH2 may serve as more critical targets for rutin-related ferroptosis in hepatocellular carcinoma cells. The expression of ACACA, AKR1C3, ALDH2, AR, and CDK1 was validated using the GSE149614 HCC single-cell dataset (Supplementary Figure 2).

Validation of Key FRTs-R Protein Expression Levels in Clinical Samples

IHC results of the protein expression of ACACA, AKR1C3, ALDH2, AR and CDK1 from HPA database were displayed in Figure 11. ACACA and AKR1C3 exhibited high expression levels in normal liver tissue and also showed elevated expression levels in HCC patients. ALDH2 was not detected in normal liver tissue but exhibited low expression levels in HCC patients. AR exhibited low expression in normal liver tissue but was not detected in HCC tissue. CDK1 was not detected in normal liver tissue but exhibited moderate expression in HCC tissue.

Molecular Docking

To investigate the mechanism of rutin-related ferroptosis in HuH-7 cells, we examined the interactions between rutin and five target proteins (ACACA, AKR1C3, ALDH2, AR, and CDK1). The specific binding characteristics were as follows: ACACA: Binding energy = −0.44 kcal/mol, forming hydrogen bonds with ARG-420 (3.4, 3.5 Å), ARG-546 (2.2, 2.5 Å), HIS-421 (2.1 Å), GLY-354 (2.0 Å), and GLY-355 (3.0 Å) (Figure 12A). AKR1C3: Binding energy = −4.5 kcal/mol, forming hydrogen bonds with ASP-78 (2.3, 2.4 Å), ARG-47 (1.9 Å), GLN-6 (2.2 Å), and GLY-13 (2.1 Å) (Figure 12B). ALDH2: Binding energy = −1.98 kcal/mol, forming hydrogen bonds with ALA-448 (1.8 Å), TRP-452 (2.3 Å), VAL-451 (2.3 Å), and VAL-458 (2.3 Å) (Figure 12C). AR: Binding energy = −2.36 kcal/mol, forming hydrogen bonds with GLN-

https://doi.org/10.2147/JHC.S560755

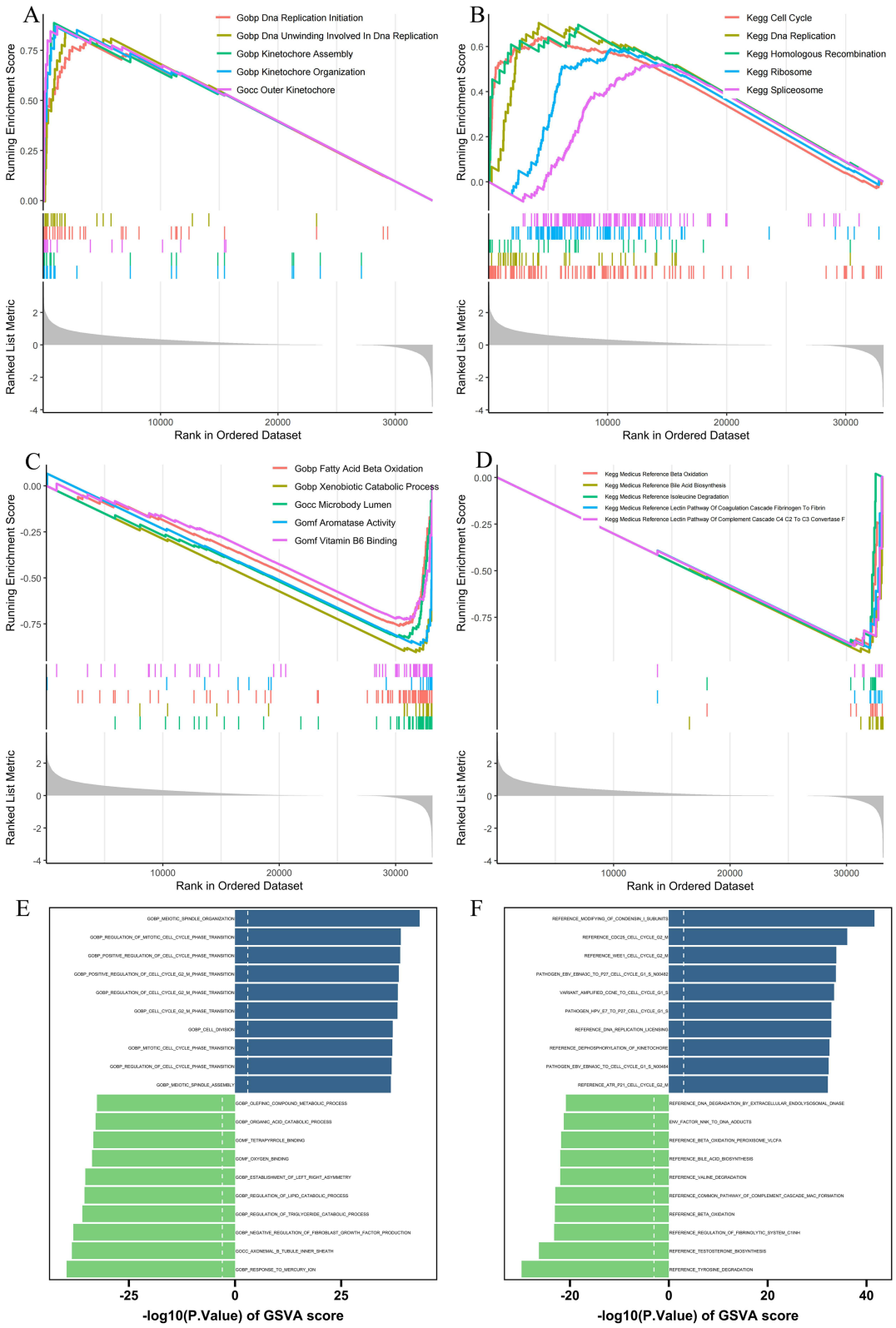

Figure 8 Gene set enrichment analysis (GSEA) and Gene set variation analysis (GSVA) between risk groups. (**A** and **B**) Top 5 upregulated pathways in GSEA analysis based on Gene Ontology (GO) and Kyoto Encyclopedia of Genes and Genomes (KEGG) gene sets; (**C** and **D**) Top 5 downregulated pathways in GSEA analysis based on GO and KEGG gene sets; (**E**) GSVA based on GO gene sets; (**F**) GSVA based on KEGG gene sets.

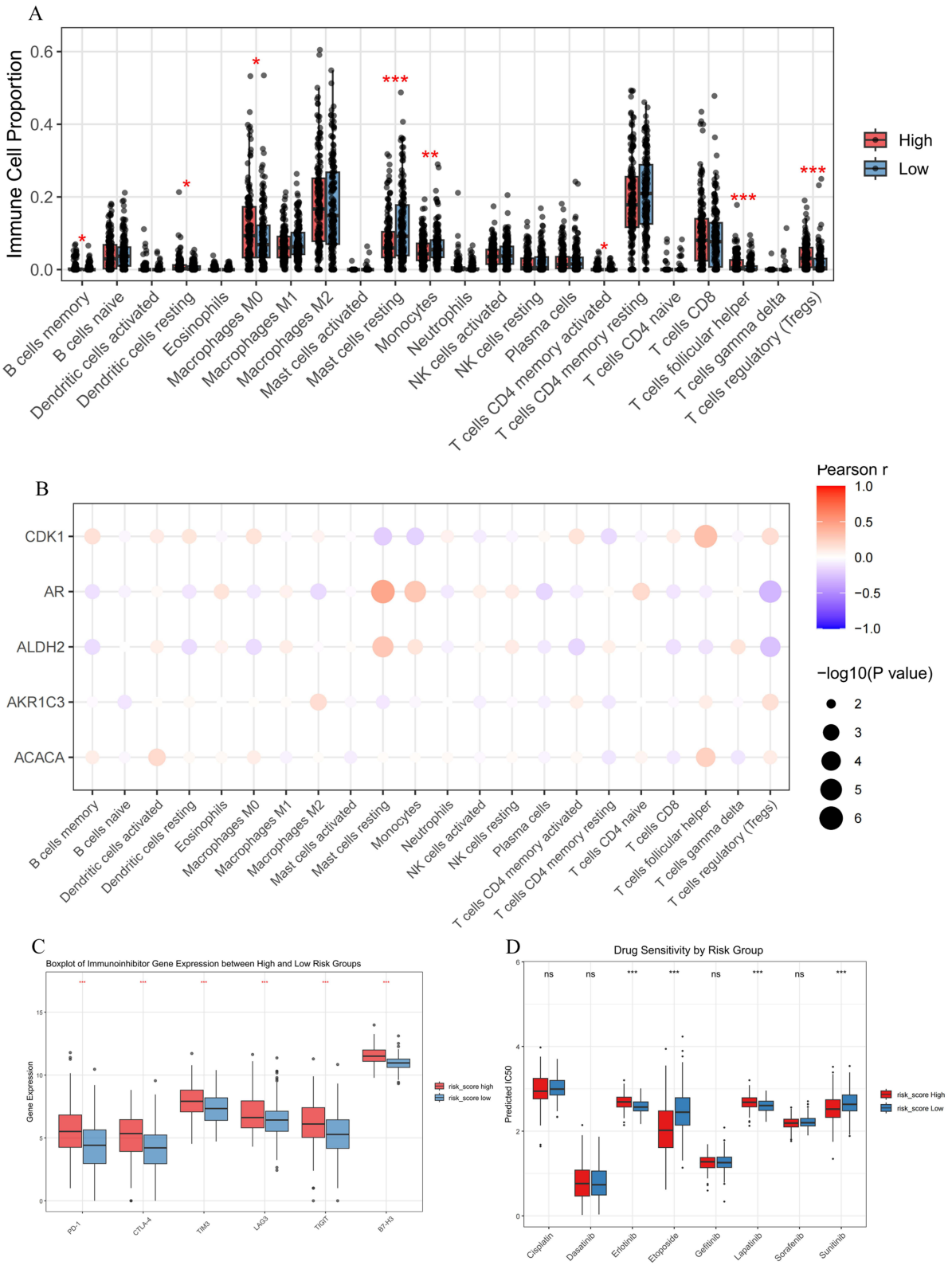

Figure 9 (**A**) Differences in various immune cells between the two risk score groups; (**B**) Correlation between hub genes and immune cells; (**C**) Expression of Immune checkpoints PD-1, CTLA-4, TIM-3, LAG-3, TIGIT, and B7-H3 in high-risk and low-risk groups of hepatocellular carcinoma patients. (**D**) Sensitivity of various chemotherapeutic and targeted agents in high- and low-risk groups of HCC patients. "*" indicates $P < 0.05$, "**" indicates $P < 0.01$ and "***" indicates $P < 0.001$.

https://doi.org/10.2147/JHC.S560755

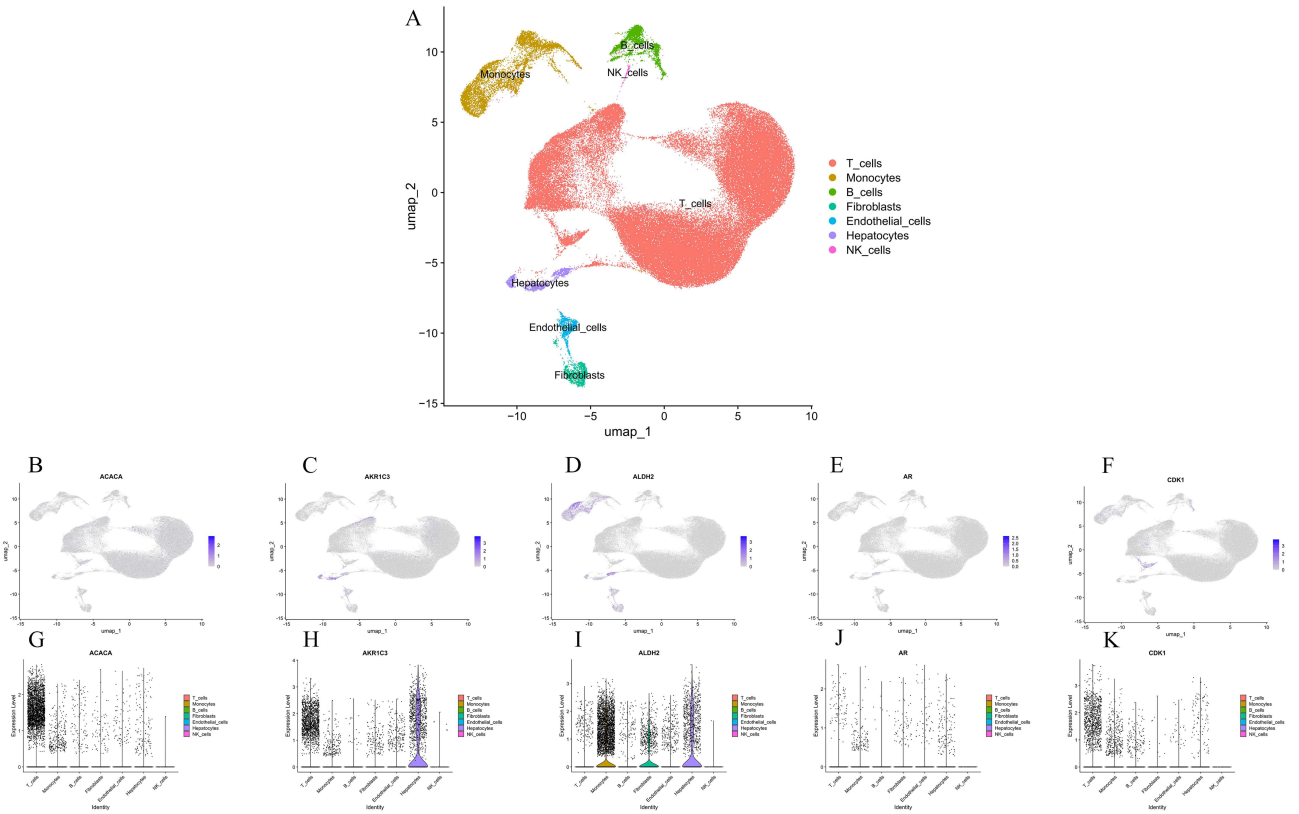

Figure 10 Single-cell analysis of rutin-related genes. (**A**) Annotation of cell subclusters in the tumor microenvironment of LIHC; (**B**–**K**) Expression pattern of the key FRTs-R in the tumor microenvironment.

919 (2.0 Å) and LYS-912 (2.3 Å) (Figure 12D). CDK1: Binding energy = −0.29 kcal/mol, forming hydrogen bonds with ASN-1453 (2.6 Å), GLN-1455 (2.0 Å), and ILE-1588 (3.1 Å) (Figure 12E). These comprehensive molecular docking results demonstrate that rutin exhibits significant binding activity with multiple target proteins (ACACA, AKR1C3, ALDH2, AR, and CDK1). Notably, the strongest binding affinity was observed with AKR1C3, suggesting that rutin may induce ferroptosis in HuH-7 cells through a multi-target synergistic mechanism, with specific inhibition of AKR1C3 potentially serving as a key mechanism.

Discussion

HCC is a prevalent and aggressive malignancy worldwide, associated with poor prognosis.[20] Current treatment options are severely limited by efficacy, safety, and cost. Despite advancements in targeted immunotherapy, challenges such as drug resistance and limited effectiveness in advanced stages persist. Therefore, in-depth exploration of HCC pathogenesis and the development of novel therapeutic strategies are of great significance. Rutin, a natural flavonoid compound abundant in fruits and traditional Chinese medicine, exhibits various pharmacological activities, including antioxidant and anti-inflammatory effects.[21,22] Prior studies indicate that the gut microbiota biotransforms rutin,[23] thereby limiting its small intestinal absorption and resulting in low oral bioavailability. To address these limitations, researchers have developed drug delivery systems—such as liposomes,[24] polymeric micelles,[25] and rutin nanoparticles[26]—to improve rutin's pharmacokinetic properties and enhance its therapeutic potential. This study demonstrates that rutin inhibits the proliferation and migration of HuH-7 cells and arrests the cell cycle. Ferroptosis, an iron-dependent, lipid peroxidation-driven cell death pathway, shows promise in HCC treatment.[27] Given the sensitivity of cancer cells to ferroptosis and their inherent defense mechanisms, identifying safe and effective ferroptosis inducers is clinically valuable. Through bioinformatics and network pharmacology, we identified 15 potential ferroptosis-related targets of rutin (FRTs-R) and constructed an HCC prognostic risk model comprising five core genes. The model revealed that the survival rate of the low-risk group was significantly better than that of the high-risk group,

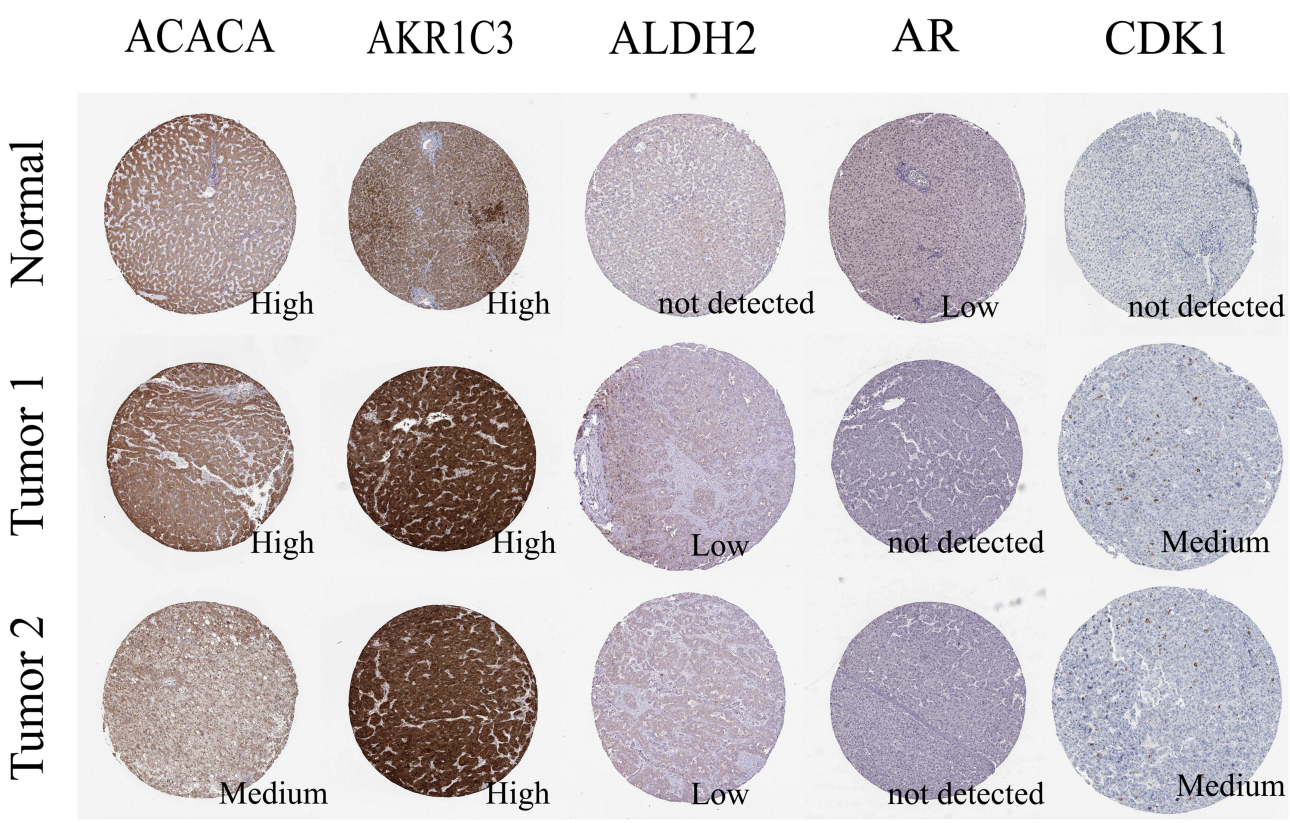

Figure 11 The protein expression levels of ACACA, AKR1C3, ALDH2, AR and CDK1 in liver tissue and hepatocellular carcinoma from the HPA online database.

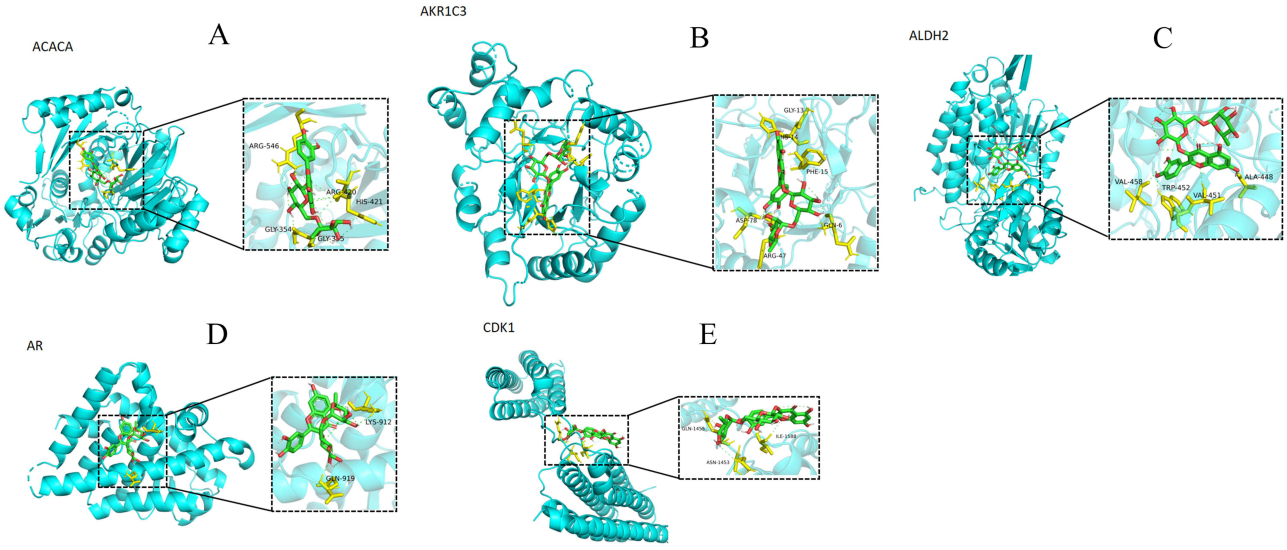

Figure 12 Molecular docking results of rutin with ACACA, AKR1C3, ALDH2, AR and CDK1. (**A**) ACACA: Binding energy = −0.44 kcal/mol, forming hydrogen bonds with ARG-420 (3.4, 3.5 Å), ARG-546 (2.2, 2.5 Å), HIS-421 (2.1 Å), GLY-354 (2.0 Å), and GLY-355 (3.0 Å). (**B**) AKR1C3: Binding energy = −4.5 kcal/mol, forming hydrogen bonds with ASP-78 (2.3, 2.4 Å), ARG-47 (1.9 Å), GLN-6 (2.2 Å), and GLY-13 (2.1 Å). (**C**) ALDH2: Binding energy = −1.98 kcal/mol, forming hydrogen bonds with ALA-448 (1.8 Å), TRP-452 (2.3 Å), VAL-451 (2.3 Å), and VAL-458 (2.3 Å). (**D**) AR: Binding energy = −2.36 kcal/mol, forming hydrogen bonds with GLN-919 (2.0 Å) and LYS-912 (2.3 Å). (**E**) CDK1: Binding energy = −0.29 kcal/mol, forming hydrogen bonds with ASN-1453 (2.6 Å), GLN-1455 (2.0 Å), and ILE-1588 (3.1 Å).

a finding that was validated in an external cohort. Additionally, we established a nomogram integrating risk scores with demographic data and clinical characteristics to aid in clinical prognosis assessment. GSEA and Gene Set Variation Analysis (GSVA) enrichment analyses indicated that ferroptosis-related pathways, such as fatty acid metabolism, were upregulated in

https://doi.org/10.2147/JHC.S560755

the low-risk group. The single-cell analysis revealed that AKR1C3 was specifically expressed in liver cancer cells, and molecular docking experiments confirmed direct binding between rutin and the key target AKR1C3, showing the most stable interactions. These findings suggest that rutin may directly induce ferroptosis in HCC cells by regulating the AKR1C3-mediated fatty acid metabolism pathway.

This study innovatively combines drug target genes and ferroptosis-related genes to assess the prognostic value in HCC.[28,29] Among the 63 differentially expressed rutin target genes (RTGs), 24% (15) were identified as FRTs-R, with five genes being recognized as key FRTs-R. Based on these genes, we developed a novel risk model to predict the overall survival of HCC patients. The model demonstrated good predictive ability in the training set and two validation sets, where the high-risk group exhibited significantly lower overall survival than the low-risk group. Furthermore, the risk scoring model was identified as an independent prognostic factor for HCC overall survival, providing potential targets for intervention. In our study, we found that among the five key FRTs-R, ACACA, AKR1C3, and CDK1 were upregulated in HCC, while AR and ALDH2 showed the opposite trend. Studies indicate that these genes play roles in ferroptosis or tumor regulation. For example, chlorogenic acid may induce ferroptosis by downregulating AKR1C3 and reprogramming arachidonic acid metabolism.[30] AKR1C3 knockdown has been shown to reduce YAP nuclear translocation and inhibit the expression of the cysteine transporter SLC7A11, ultimately leading to increased intracellular ferrous ion levels and ferroptosis induction.[31] Additionally, AKR1C3 knockout inhibited the Akt pathway, increasing reactive oxygen species, which may subsequently reduce HCC cell proliferation by promoting ferroptosis. Thus, targeting AKR1C3 may represent a promising strategy to overcome sorafenib resistance.[32,33] CDK1 directly binds to and phosphorylates serine 447 (S447) on long-chain fatty acyl-CoA synthetase 4 (ACSL4), leading to ACSL4 protein degradation. The reduction in ACSL4 blocked the biosynthesis of lipids containing polyunsaturated fatty acids, thereby inhibiting lipid peroxidation and ferroptosis.[34] ACACA, as a key regulator and rate-limiting enzyme in lipid synthesis and oxidation, has been identified as an attractive target for HCC in several studies.[35,36] Since iron-dependent phospholipid peroxidation drives ferroptosis, the role of ACACA in HCC ferroptosis is equally important. Additionally, AR alters liver cancer invasion by indirectly inhibiting NF-κB.[37] These results suggest that AR may inhibit metastasis in advanced liver cancer. ALDH2 belongs to the aldehyde dehydrogenase family and plays an important role in the redox reactions of ethanol and endogenous aldehyde products released from lipid peroxidation. Hepatocellular carcinoma patients with high ALDH2 expression are associated with good prognosis.[38] These results suggest that these 5 key FRTs-*Rs* do play an important role in rutin-related ferroptosis in liver cancer cells.

We explored the role of key FRTs-R in HCC from multiple perspectives. HCC patients were categorized into low-risk and high-risk groups based on a risk model. GSEA and GEVA revealed that metabolic pathways related to substance metabolism, including fatty acid β-oxidation, fatty acid catabolism, and oxidoreductase activity, were upregulated in the low-risk group. Uncontrolled lipid peroxidation is a hallmark of ferroptosis; when phospholipid peroxides accumulate to a certain threshold, they can cause rapid and irreversible damage to cell membranes, ultimately leading to ferroptosis.[39] Overall survival was significantly higher in the low-risk group than in the high-risk group, likely because liver cancer cells in the low-risk group were more susceptible to ferroptosis, thereby positively influencing patient prognosis. Recent studies have revealed a close relationship between ferroptosis and anti-cancer immunity, prompting further investigation into whether key FRTs-R affect immune infiltration in the tumor microenvironment of liver cancer. Notably, the number of resting dendritic cells was significantly lower in the low-risk group than in the high-risk group, while the M1/M2 ratio was relatively high; the numbers of regulatory T cells and follicular helper T cells were also lower. This phenomenon may relate to the release of various immunostimulatory signals by cancer cells in the early stages of ferroptosis, promoting the activation of dendritic cells and driving macrophage polarization from the M2 to M1 phenotype, thereby enhancing anti-tumor immunity.[40,41] This observation also explains the significant positive correlation between the expression level of AKR1C3, a known ferroptosis suppressor gene in HCC, and M2 cells. Regulatory T cells can hinder effective anti-tumor immune surveillance; thus, inhibiting GPX4 in Treg cells can enhance anti-tumor immune responses. Furthermore, since follicular helper T cells exhibit high susceptibility to ferroptosis,[42,43] this may account for their lower proportion in the low-risk group. Additionally, the expression levels of immune checkpoint genes, including PD-1, CTLA-4, TIM-3, LAG-3, TIGIT, and B7-H3, were higher in the high-risk group. This observation aligns with prior studies, suggesting that elevated immune cell infiltration may indicate the potential for immunotherapy, such as immune

checkpoint inhibitors.[44] Drug sensitivity analysis indicated that patients in different risk groups exhibited varying sensitivities to chemotherapeutic drugs, which may improve the selection of immune checkpoint inhibitors and chemotherapeutic agents for HCC patients. Single-cell analysis and molecular docking results indicated that only AKR1C3 and ALDH2 were primarily expressed in hepatocytes, with AKR1C3 demonstrating the most stable binding with rutin, consistent with prior research. Human AKR1C3 can catalyze the production of 9α,11β-PGF_2 from PGD_2 in the presence of NADPH. Since rutin occupies the same site where PGD_2 binds to AKR1C3, it may act as an inhibitor of AKR1C3.[45] This suggests that rutin could induce ferroptosis in liver cancer cells by binding to AKR1C3, offering new insights for targeted therapies aimed at reducing the side effects of chemotherapy in the future.

However, this study has several limitations. First, the findings are primarily based on in vitro models, which lack validation in in vivo mouse models, limiting the assessment of their physiological relevance. Second, our investigation focused solely on the effects of rutin on HCC cell proliferation, cell cycle, metastasis, and invasion; we did not definitively establish whether rutin promotes tumor cell death through specific mechanisms such as ferroptosis, apoptosis, autophagy, or pyroptosis, or a combination of these pathways. Nevertheless, this study employed bioinformatics and network pharmacology approaches to predict that rutin may primarily inhibit the occurrence and progression of HCC by regulating AKR1C3-mediated ferroptosis. These findings provide a theoretical basis for further exploration of the molecular mechanisms of rutin in cancer intervention and suggest directions for future research.

Conclusions

In conclusion, we have validated the significant efficacy of rutin in combating liver cancer cells. Additionally, we developed a novel risk scoring model based on FRTs-R, which demonstrates superior performance in prognostic prediction. Bioinformatics analysis suggests that Rutin may affect ferroptosis in HCC cells by regulating lipid metabolism through the action of AKR1C3. Our research provides new insights into the mechanisms by which FRTs-R regulate the HCC immune microenvironment and drug resistance. These findings may serve as an important reference for future therapeutic strategies and personalized medicine approaches targeting HCC.

Institutional Review Board Statement

The research content of this manuscript does not involve human participants, so institutional review board approval was not required.

Data Sharing Statement

All data generated or analyzed during this study are included in this published article and its supplementary information files. The original data will be available upon reasonable request to the corresponding authors.

Ethics Statement

According to Article 32, Paragraphs 1 and 2 of the "Measures for Ethical Review of Life Science and Medical Research Involving Human Subjects", released on February 18, 2023: (1) Research utilizing legally obtained public data or data generated through observation without interfering with public behavior; (2) Research using anonymized information data, may be exempt from ethical review.

Funding

This work was supported by the Public Welfare Foundation of Zhejiang Science and Technology Agency, No. LGF22H160047; Zhejiang Medical and Health Science and Technology Plan Project, No. 2021436629; Zhejiang Province Traditional Chinese Medicine Science and Technology Project, No. 2023ZL317.

Disclosure

The authors declare that they have no conflicts of interest for this work.

References

1. Sung H, Ferlay J, Siegel RL, et al. Global cancer statistics 2020: GLOBOCAN estimates of incidence and mortality worldwide for 36 cancers in 185 countries. *CA*. 2021;71(3):209–249. doi:10.3322/caac.21660
2. Jun JM, Geetha Gopalakrishna P, Carlos Jose A, et al. Integrative oncology: addressing the global challenges of cancer prevention and treatment. *CA*. 2021;72(2):144–64.
3. Alejandro F, María R, Jordi B. Hepatocellular carcinoma. *Lancet*. 2018;391(10127).
4. Moris D, Martinino A, Schiltz S, et al. Advances in the treatment of hepatocellular carcinoma: an overview of the current and evolving therapeutic landscape for clinicians. *CA*. 2025;75(6):498–527. doi:10.3322/caac.70018
5. Josep ML, Florian C, Mathias H, et al. Immunotherapies for hepatocellular carcinoma. *Nat Rev Clin Oncol*. 2021;19(3):151–72.
6. Mengke W, Hanning L, Yuxin L, Yang S. Research progress on the mechanisms of traditional chinese medicine in preventing and treating HCC invasion and metastasis based on lipid metabolic reprogramming. *Curr Top Med Chem*. 2025.
7. Nikfarjam BA, Adineh M, Hajiali F, Nassiri-Asl M. Treatment with Rutin - A therapeutic strategy for neutrophil-mediated inflammatory and autoimmune diseases: - anti-inflammatory effects of rutin on neutrophils. *J Pharmacopuncture*. 2017;20(1):52–56. doi:10.3831/KPI.2017.20.003
8. Ganeshpurkar A, Saluja AK. The pharmacological potential of rutin. *Saudi Pharm J*. 2017;25(2):149–164. doi:10.1016/j.jsps.2016.04.025
9. Chen H, Miao Q, Geng M, et al. Anti-tumor effect of rutin on human neuroblastoma cell lines through inducing G2/M cell cycle arrest and promoting apoptosis. *ScientificWorldJournal*. 2013;2013:269165. doi:10.1155/2013/269165
10. Perk AA, Shatynska-Mytsyk I, Gerçek YC, et al. Rutin mediated targeting of signaling machinery in cancer cells. *Cancer Cell Int*. 2014;14(1):124. doi:10.1186/s12935-014-0124-6
11. Zhou M, Zhang G, Hu J, et al. Rutin attenuates sorafenib-induced chemoresistance and autophagy in hepatocellular carcinoma by regulating BANCR/miRNA-590-5P/OLR1 axis. *Int J Biol Sci*. 2021;17(13):3595–3607. doi:10.7150/ijbs.62471
12. Chen J, Li X, Ge C, Min J, Wang F. The multifaceted role of ferroptosis in liver disease. *Cell Death Differ*. 2022;29(3):467–480. doi:10.1038/s41418-022-00941-0
13. Liu W, Zhu Y, Ye W, et al. Redox regulation of TRIM28 facilitates neuronal ferroptosis by promoting SUMOylation and inhibiting OPTN-selective autophagic degradation of ACSL4. *Cell Death Differ*. 2025;32(6):1041–1057. doi:10.1038/s41418-025-01452-4
14. Sun Y, Fang G, Liu K, et al. Natural polyphenol rutin inhibits ferroptosis in ulcerative colitis by regulating lipid metabolism via blocking the LCN2-ALOX15 axis. *Food Funct*. 2025;16(18):7169–7186. doi:10.1039/D5FO01220A
15. Chen S, Li Z, Xiao Y, Zhou Z, Zhan Q, Yu L. Rutin targets AKT to inhibit ferroptosis in ventilator-induced lung injury. *Phytother Res*. 2024;38(7):3401–3416. doi:10.1002/ptr.8212
16. Du Y, Guo Z. Recent progress in ferroptosis: inducers and inhibitors. *Cell Death Discov*. 2022;8(1):501. doi:10.1038/s41420-022-01297-7
17. Diao J, Jia Y, Dai E, et al. Ferroptotic therapy in cancer: benefits, side effects, and risks. *Mol Cancer*. 2024;23(1):89. doi:10.1186/s12943-024-01999-9
18. Lee S, Lee J, Lee H, Sung J. Relative protective activities of quercetin, quercetin-3-glucoside, and rutin in alcohol-induced liver injury. *J Food Biochem*. 2019;43(11):e13002. doi:10.1111/jfbc.13002
19. Thushina EN, Mustafina OK, Kravchenko LV, Balakina AS, Alekseeva IA, Riger NA. Effect of minor bioactive food substances – rutin and hesperidin in their separate and combined alimentary arrives on the immune system of rats and the activity of nuclear factor NF-kB liver cells. *Vopr Pitan*. 2015;84(6):19–29.
20. Bray F, Laversanne M, Sung H, et al. Global cancer statistics 2022: GLOBOCAN estimates of incidence and mortality worldwide for 36 cancers in 185 countries. *CA*. 2024;74(3):229–263. doi:10.3322/caac.21834
21. Ghaffar AA, Radwan RR, A HE. Radiation synthesis of poly(Starch/Acrylic acid) pH sensitive hydrogel for rutin controlled release. *Int J Biol Macromol*. 2016;92:957–64.
22. Jie-Qiong M, Chan-Min L, Wei Y. Protective effect of rutin against carbon tetrachloride-induced oxidative stress, inflammation and apoptosis in mouse kidney associated with the ceramide, MAPKs, p53 and calpain activities. *Chem Biol Interact*. 2018;286:26–33.
23. Manach C, Morand C, Demigné C, Texier O, Régérat F, Rémésy C. Bioavailability of rutin and quercetin in rats. *FEBS Lett*. 1997;409(1):12–16. doi:10.1016/S0014-5793(97)00467-5
24. Li Z, Liang S, Sun H, Bao C, Li Y. Antilipogenesis effect of rutin-loaded liposomes using a microneedle delivery system. *ACS Appl Mater Interfaces*. 2023;15(47):54294–54303. doi:10.1021/acsami.3c12795
25. Ibrahim R, Kasabri V, Sunoqrot S, Shalabi D, Alkhateeb R, Alhiari Y. Preparation and characterization of rutin-encapsulated polymeric micelles and studies of synergism with bioactive benzoic acids and triazolofluoroquinolones as anticancer nanomedicines. *Asian Pac J Cancer Prev*. 2023;24(3):977–989. doi:10.31557/APJCP.2023.24.3.977
26. Wu H, Su M, Jin H, et al. Rutin-loaded silver nanoparticles with antithrombotic function. *Front Bioeng Biotechnol*. 2020;8:598977. doi:10.3389/fbioe.2020.598977
27. Chang WT, Bow YD, Fu PJ, et al. A marine terpenoid, heteronemin, induces both the apoptosis and ferroptosis of hepatocellular carcinoma cells and involves the ROS and MAPK pathways. *Oxid Med Cell Longev*. 2021;2021:7689045. doi:10.1155/2021/7689045
28. Jie-Ying L, De-Shen W, Hao-Cheng L, et al. A novel ferroptosis-related gene signature for overall survival prediction in patients with hepatocellular carcinoma. *Int J Biol Sci*. 2020;16(13):2430.
29. Tianxing D, Jing L, Xu L, et al. Prognostic role and potential mechanisms of the ferroptosis-related metabolic gene signature in hepatocellular carcinoma. *Pharmgenomics Pers Med*. 2021;14:927–45.
30. Ling W, Hong-Yao C, Jing-Ting Z, et al. Chlorogenic acid induces hepatocellular carcinoma cell ferroptosis via PTGS2/AKR1C3/GPX4 axis-mediated reprogramming of arachidonic acid metabolism. *World J Gastrointest Oncol*. 2025;17(3):98844.
31. Jinsi C, Jia Z, Wei T, et al. AKR1C3 suppresses ferroptosis in hepatocellular carcinoma through regulation of YAP/SLC7A11 signaling pathway. *Mol Carcinog*. 2023;62(6):833–44.
32. Chenghui Z, Zhefang W, Jiahui L, et al. Aldo-keto reductase 1C3 mediates chemotherapy resistance in esophageal adenocarcinoma via ROS detoxification. *Cancers*. 2021;13(10):2403.
33. Jia Z, Zhihong Y, Yanlei L, Li Y, Ruili Y. Knockdown of AKR1C3 promoted sorafenib sensitivity through inhibiting the phosphorylation of AKT in hepatocellular carcinoma. *Front Oncol*. 2022;12:823491.

34. Kaixuan Z, Weihao L, Yue W, et al. Inhibition of CDK1 overcomes oxaliplatin resistance by regulating ACSL4-mediated ferroptosis in colorectal cancer. *Adv Sci*. 2023;10(25):2301088.
35. Robert US, Seth JP, Lillian JE, et al. Inhibition of acetyl-CoA carboxylase suppresses fatty acid synthesis and tumor growth of non-small-cell lung cancer in preclinical models. *Nat Med*. 2016;22(10):1108–19.
36. Philipp KH, Florian C, Miguel T-M, et al. Molecular markers of response to anti-PD1 therapy in advanced hepatocellular carcinoma. *Gastroenterology*. 2022;164(1):72–88.
37. Wen-Lung M, Cheng-Lung H, Chun-Chieh Y, et al. Hepatic androgen receptor suppresses hepatocellular carcinoma metastasis through modulation of cell migration and anoikis. *Hepatology*. 2012;56(1):176–85.
38. Guojun H, Lei C, Gang L, et al. Aldehyde dehydrogenase-2 (ALDH2) opposes hepatocellular carcinoma progression by regulating AMP-activated protein kinase signaling in mice. *Hepatology*. 2016;65(5):1628–44.
39. Xuejun J, Brent RS, Marcus C. Ferroptosis: mechanisms, biology and role in disease. *Nat Rev Mol Cell Biol*. 2021;22(4):266–82.
40. Iuliia E, Elena C, Louis V, et al. Vaccination with early ferroptotic cancer cells induces efficient antitumor immunity. *J Immunother Cancer*. 2020;8(2):e001369.
41. Bo Y, Bongseo C, Weiguo L, Dong-Hyun K. Magnetic field boosted ferroptosis-like cell death and responsive MRI using hybrid vesicles for cancer immunotherapy. *Nat Commun*. 2020;11(1):3637.
42. Chengxian X, Shaogang S, Travis J, et al. The glutathione peroxidase Gpx4 prevents lipid peroxidation and ferroptosis to sustain Treg cell activation and suppression of antitumor immunity. *Cell Rep*. 2021;35(11).
43. Yin Y, Zhian C, Hao Z, et al. Author Correction: selenium-GPX4 axis protects follicular helper T cells from ferroptosis. *Nat Immunol*. 2024;25(9):1599–600.
44. Uasim H, Miriam W, Pranavan P, Craig M, Lionel H. Immune checkpoint inhibitors in HCC: cellular, molecular and systemic data. In: *Seminars in Cancer Biology*. Elsevier; 2022: 799–815.
45. Junichi K, Taro Y, Kikuko W, Fusao T. Crystal structure of human prostaglandin F synthase (AKR1C3). *Biochemistry*. 2004;43(8).